THE JOURNAL OF PHYSICAL CHEMISTRY C

Article

pubs.acs.org/JPCC

Real-Time Monitoring Distance Changes in Surfactant-Coated Au Nanoparticle Films upon Volatile Organic Compounds (VOCs)

M. C. Dalfovo, L. J. Giovanetti, J. M. Ramallo-López, R. C. Salvarezza, F. G. Requejo, and F. J. Ibañez*

Instituto de Investigaciones Fisicoquímicas, Teóricas y Aplicadas (INIFTA), Universidad Nacional de La Plata - CONICET, Sucursal 4 Casilla de Correo 16, 1900 La Plata, Argentina

Supporting Information

ABSTRACT: We explore into the role of the organic ligands composition surrounding Au nanoparticles (NPs) toward internanoparticles distance changes and film structure during vapor sensing by the use of *in situ* grazing-incidence small-angle X-ray scattering (GISAXS) and other relevant techniques. We observed distinct changes in *core-to-core* distance and film structure upon measured concentrations of polar ethanol (EtOH) and nonpolar toluene (Tol) vapors. As-formed tetraoctylammonium bromide (TOABr)-coated Au NPs (SNPs) film exhibited ∼0.4 nm core-to-core increase in distance and improved SNPs correlation upon 80% Tol. In the presence of EtOH, SNPs distance seems not to change and correlation critically diminishes, leading to an amorphous film. As-formed films were exchanged with nonanedithiol (NDT) and exposed to 100% Tol vapor. Interestingly, the incorporation of NDT increased distance between NPs and rendered film flexibility. It is determine that just a small number of S, from NDT ligands, binds to Au NPs, and those exchanged alkanedithiol chains adopted a loop conformation around the Au NPs as evidenced by X-ray absorption near-edge structure (XANES) and kink defects by Fourier transformed infrared (FT-IR) experiments, respectively. These findings may solve some fundamental questions about internanoparticle distance-dependent phenomena such as electron transport in chemiresistors and coupling effects in localized surface plasmon resonance (LSPR) solid-state sensors.

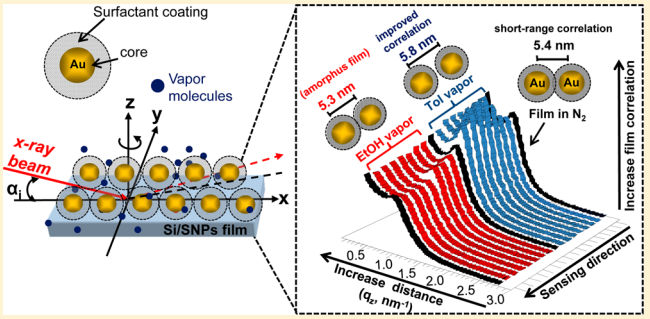

INTRODUCTION

To correlate changes in distance between nanoparticles (NPs) with conductivity (i.e., electron hopping or tunnel) and coupling effects in chemiresistive and localized surface plasmon resonance (LSPR) sensors, respectively, is fundamentally important to better understand some phenomena that occur at the nanoscale. In the applied field, it is also relevant to control the internanoparticles distance (inter-NPd) between metal cores for improvements in solar cells,[1] surface-enhanced Raman scattering (SERS),[2] and detection of volatile organic compounds (VOCs) or gases via chemiresistive sensing,[3] just to mention a few. An organic-coated metal NPs film could be an ideal platform because metallic cores provide the analytical signal, while the organic matrix may act as a flexible receptor for the incoming vapor analytes. The presence of VOCs may alter either or both main variables in a metal−organic film: *core-to-core* distance and/or dielectric of the surrounding medium. In most cases the former parameter is assumed to dominate the detection mechanism; however, it has never been conclusively determined. The extent to which the signal changes depends on the chosen transducing method. For instance, a chemiresistor[3] is a type of sensitive film that, at room temperature, exponentially changes resistivity upon changes in internano-particle distance (inter-NPd) and dielectric via an activated *core-to-core* electron hopping mechanism.[4,5] On the other hand, plasmon sensors commonly rely on linearly dependent changes between the plasmon band and refractive index (RI) according to the Mie theory.[6] The exponential distance dependence toward changes in film resistance explains why chemiresistive sensors have been extensively used in the detection of VOCs.[7−12] Although it is true that chemiresistors are sensitive, they lack of selectivity because changes in film resistance commonly occurs in the same direction (either increases or decreases) regardless of the nature of the vapor analyte.[3,13−15]

Recently, plasmon sensors built with organic-coated NPs films have gained important attention toward the detection of vapor analytes[16−20] likely due to their ability to discriminate between headspace nonpolar and polar vapors by distinct shifts of the plasmon band toward blue and red, respectively.[18] We attributed the blue plasmon shift to film swelling[18] (nano-particles separation) overriding the expected red-shift caused by an increase in RI by Tol. Scholten et al. later demonstrated distinct blue-shifts upon Tol and *n*-heptane vapors of a film composed of *n*-octanethiolate Au NPs.[19] While blue-shifts were attributed to swelling counteracting the increase in RI (red-shift), a significant red-shift observed upon EtOH vapor[18] was

Received: November 3, 2014
Revised: January 7, 2015
Published: February 10, 2015

DOI: 10.1021/jp511014q
J. Phys. Chem. C 2015, 119, 5098−5106

attributed to a cooperation between film compaction (NPs approaching) and increase in RI. In our paper[18] and others,[7,19,21,22] it has been usually speculated that an overall film swelling- or compaction-induced mechanisms are predominant; however, *in situ* measurements regarding inter-NPd changes upon VOCs are still challenging with microscopes.

A powerful technique such as grazing incidence small-angle X-ray scattering (GISAXS) provides *real-time* information about inter-NPd and film structure. In a recent perspective by Goodfellow and Korgel,[23] it was emphasized on the importance of exploring forces that control self-assembly, supercrystal structures, and structural changes in NPs films during solvent or vapor annealing. Nanoparticles correlation has been usually achieved by monolayer-protected clusters (MPCs) where the organic chains are well assembled around the surface, and the distance between cores is precisely controlled by the length of the organic ligands. For instance, Zhang et al. performed *in situ* GISAXS evolution for studying structural changes in drop-casted oleic acid- and oleylamine-coated Pt_2Cu_3 MPC films during vapor drying.[24] They demonstrated that the order of the film could be significantly improved by retarding the kinetics of hexane evaporation (film drying) as compared to drop-cast films whose evaporation occurs at much faster rate. In most cases, the literature has shown that a 3D crystalline film is readily achieved after solvent evaporation[25] as demonstrated in GISAXS[26,28] and small-angle X-ray scattering (SAXS)[27,29] experiments. Hanrath and co-workers observed that the concentration of ligands also plays a fundamental role in film order.[30] They determined that, as long as density of ligands decreases, the film became more disordered restructuring from a body-centered cubic (bcc) into a face-centered cubic (fcc). Other variables such as temperature and UV irradiation have been shown to decrease inter-NPd in 3.5 nm organic-coated PbS NPs[31] and oleic acid- and oleylamine-coated Pt_2Cu_3 NPs nanoparticle films.[24] Pileni and co-workers demonstrated reversible inter-NPd changes by the use of *in situ* small-angle X-rays diffraction (SAXRD).[29] They showed ∼1.0 nm distance increase for 1-dodecanethiol-coated (C12S) Au MPCs film upon 75% Tol concentration.

In the present work, we demonstrate for the first time distinct changes in *core-to-core* distance and film restructuring for surfactant- and nonanedithiol NDT-treated Au nanoparticles (SNPs) films exposed to known concentrations of polar and nonpolar vapors by the use of *real-time* GISAXS. In order to attain correlation, an APTES-functionalized Si substrate was immersed into toluene-containing SNPs. This approach exhibited short-range correlation and distinct behavior in the presence of Tol and EtOH vapors similar to recently reported LSPR sensors.[18] We employed complementary techniques such as XANES, FT-IR, UV−vis, and cyclic voltammetry (CV) in order to explore into the Au−SR interaction and its effects on sensing. These results shed light onto fundamental aspects in VOCs sensing such as the role of the organic coating, film deposition and order, nanoparticles distance, film flexibility, and alkyl chain conformation around the metal cores.

EXPERIMENTAL SECTION

Synthesis of Surfactant-Coated Au Nanoparticles (SNPs). The TOABr-coated Au NPs (SNPs) were synthesized according to the modified two-phase Brust−Schiffrin reaction but without the addition of alkanethiols as previously reported.[32] The SNPs prepared in this manner are 2.9 ± 0.6 nm in diameter according to small-angle X-ray scattering (SAXS) fitted curves of SNPs dispersed in toluene solution.

Nanoparticles Film Assembly. In order to obtain correlation, SNPs films were assembled by two different approaches. Silicon (100) substrates were cleaned with piranha solution, rinsed with nanopure water and ethanol, and dried under N_2 flow. These substrates were later functionalized with 3-aminopropyltrilethoxysilane (APTES) by placing the samples into a solution containing 10 mL of ethanol, 100 μL of APTES, and 2−3 drops of nanopure water. The solution was heated just once at 70 °C for 10 min, and the substrates were further incubated for 1 h at ambient temperature. The functionalized Si substrates were sonicated in ethanol and dried under N_2 flow. Film deposition was carried out either by drop-casting 30 μL from a 1.1 mg/mL NPs solution into the functionalized Si substrate or by immersion of an APTES-functionalized Si substrate into a freshly prepared SNPs solution for 37 h. The letter deposition method exhibited SNPs correlation sufficient for further GISAXS analysis.

Film Treatment with Thiols and Dithiols. A correlated SNPs film obtained by immersion named "as-formed" were liquid-phase place-exchanged by immersion into 20 mM 1,9-nonanedithiol (NDT) and 1-nonanethiol (NT) hexane solution for 2 h except for films used in FT-IR experiments. Vapor-phase place-exchanged reaction was conducted by placing 1 mL of the exchange thiol in a vial cap which was further isolated inside a Petri dish along with the SNPs film for 2 h. After exchange, samples were copiously rinsed with hexane and dried under N_2 flow. As-treated films were used as a control experiment in GISAXS and SAXS experiments.

***In Situ* GISAXS Sensing.** All X-rays experiments were carried out at the Brazilian Synchrotron Light Laboratory (LNLS) in Campinas, Brazil. GISAXS employed the XRD2 X-ray diffraction beamline with a wavelength (λ) and incidence angle (α_i) set up at 0.1550 nm and 0.3°, respectively. The scattered photons were recorded (100 s/frame) using a Pilatus 2D position sensitive detector. Nanoparticle films were place in an ad-hoc gas chamber and exposed to alternating flows of pure N_2 and different concentrations of Tol and EtOH obtained by mixing N_2 with the aforementioned vapors. Varied concentrations of vapors were obtained using two mass flow controllers (MFCs) (model SLA5850, Brooks Instruments Secondary Electronics) with 5−500 mL/min flow range. MFCs were located between the N_2 cylinder and the gas chamber (see Figure S3 in Supporting Information). One line was pure N_2, and the other bubbled trough the solvent of interest. The as-formed SNPs film was exposed to 20, 40, 80, and 100% vapor concentration over a total flow of 50 mL/min. Saturated Tol and EtOH vapors were run at low (50 mL/min), middle−low (100 mL/min), middle (200 mL/min), and high (500 mL/min) total flows. Each step corresponds to an average of five measured frames chosen before vapor "off".

Other Characterization Techniques. *SAXS:* SAXS measurements were obtained using the SAXS-1 beamline. The SAXS intensity curves were determined using a 2D Pilatus detector as functions of the modulus of the scattering vector $q = 4\pi \sin\theta/\lambda$, θ being half the scattering angle and λ the X-ray wavelength, λ = 1.61 Å. The SAXS curves were normalized to the intensity of the direct X-ray beam to compensate for the continuous decrease in emission of the synchrotron source. The solid-state films under study were placed inside a cell with two thin and parallel mica windows for transmission SAXS measurements and run under air and solvents of EtOH and

DOI: 10.1021/jp511014q
J. Phys. Chem. C 2015, 119, 5098−5106

Tol. *XANES*: These experiments were performed at the SXS beamline. XANES spectra were obtained at the S K-edge (2472 eV). Details of the experimental setup have been published elsewhere.[33] The X-ray absorption spectra were recorded in fluorescence mode following sulfur Kα_1 (2309.5 eV) and Kα_2 (2308.4 eV) fluorescent emission lines as a function of photon incident energy. The XANES spectra were background subtracted and normalized to the postedge intensity. *FT-IR*: FT-IR experiments were acquired in a Nicolet 380 (USA) in transmission mode. KBr disks were gently cleaned with toluene previous to drop-cast deposition of 60 μL from a 1.1 mg/mL NPs solution. As-deposited films were thiol-treated in the vapor phase as indicated followed by copious rinsing with hexane unless indicated. Each spectrum was normalized to the intensity of the umbrella (U) peak at ~1377 cm^{-1} used as an internal yardstick.[34] *UV−vis*: UV−vis experiments were run in a PerkinElmer Lambda 35 spectrophotometer at a wavelength range from 300 to 900 nm. We performed UV−vis of these films in dry air by the presence of absorbing silica gel. Glass substrates were cleaned and functionalized the same manner as GISAXS substrates.

RESULTS AND DISCUSSION

Film Assembly and Correlation. Chemically synthesized TOABr-coated Au nanoparticles (SNPs) dispersed in toluene (Tol) exhibited 2.9 ± 0.6 nm diameter and no spatial correlation[35] according to small-angle X-ray scattering (SAXS) fitted curves (Figure S1, Supporting Information). The lack of correlation implies that the majority of entities are unevenly separated as expected to occur for SNPs dispersed in solution. In order to obtain correlation and later perform GISAXS sensing, SNPs were assembled as solid-state films by either drop-cast deposition or immersion (see Experimental Section for more details). Figure 1A,B shows GISAXS patterns, GISAXS profiles (cuts along q_z), and cartoons representing the outcome from both deposition methods as indicated. GISAXS correlation provides insights into inter-NPd and overall film organization on the basis of NPs spatial arrangement along the parallel (q_y) and perpendicular (q_z) axes to the substrate surface. Surprisingly, the drop-cast approach exhibited no GISAXS pattern indicating the lack of spatial correlation. Figure 1B, on the other hand, exhibits short-range correlation, which is evidenced by an annular halo in the image and the evolved peak at q_z in the plot. The absence of SNPs correlation could be associated with some degree of disorder caused by large amount of detergent and the chosen deposition method. Significant phase segregation or boundaries in drop-coated SNPs films has already been observed by SEM[15] and later confirmed by FT-IR experiments,[18] which exhibited micelle-like structures and significant alky chain gauche defects, respectively, relative to well-organized and strongly chemisorbed alkanethiols (i.e., C6S Au MPCs). Lack of correlation could also be attributed to the kinetics of film formation (solvent evaporation).[24] While drop-casted films were formed in few seconds, an APTES-modified substrate was immersed in toluene-containing SNPs for ~37 h. Consistent with GISAXS, nanoparticles disorder (poor correlation) has also been observed with SAXS experiments performed on drop-casted SNPs film (Figure S2). The broad along with poorly defined scattering peak (q) makes difficult any estimation of the actual distance between SNPs. These findings oppose what is reported in the literature for drop-cast films. For instance, drop-casted C12S Ag[27] and Au MPCs[36] revealed a crystalline

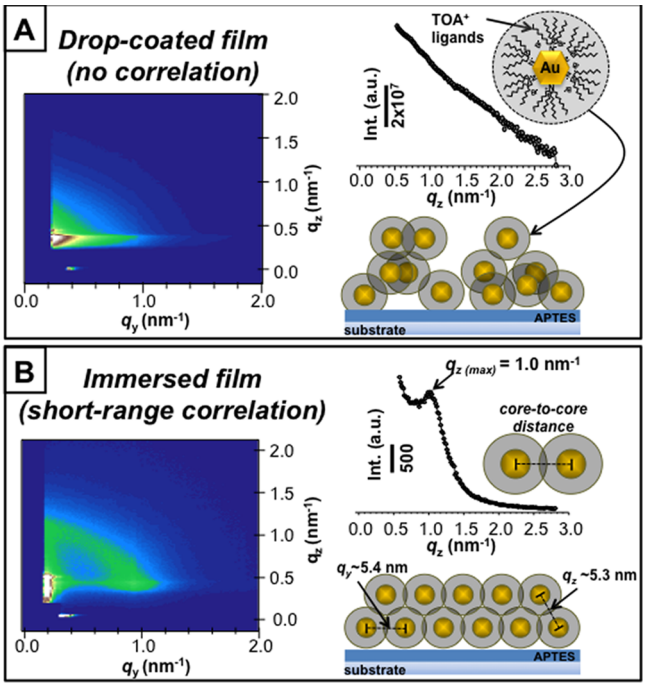

Figure 1. GISAXS pattern and intensity profiles (cuts along q_z) of drop-coated (A) and immersed (B) surfactant-coated Au NPs (SNPs) onto/into APTES-functionalized Si substrate along with cartoons representing the outcome from both film assemblies.

structure as soon as the solvent evaporated from the film as determined by SAXS and small-angle X-ray diffraction (SAXRD) experiments, respectively. There are also some discrepancy about the technique employed for measuring NPs size and inter-NPd. As an example, SAXS and TEM experiments performed on drop-casted C12S Ag MPCs on mica exhibited ~2.1 and 1.6 nm *edge-to-edge* distance, respectively.[27] Our SAXS (Figure S2) and previous TEM data[18] for drop-cast deposited SNPs on mica and Cu grid, respectively also exhibited relatively shorter distances when using the latter technique. Accordingly, there are few variables that affect inter-NPd and film structure,[28] and those may include the nature of the organic ligands, type of substrate, deposition method, and the characterization technique employed in these experiments.[26,31,37,38] Nevertheless, films assembled by immersion exhibited short-range correlation sufficient for further GISAXS analysis.

Internanoparticles Distance in Correlated SNPs. According to a semiempirical model derived from the Born−Green approximation and described by Guinier,[39] it is possible to estimate the average *core-to-core* distance (d) between entities (nanoparticles) by using the expression

$$d = 5.6/q_{max} \quad (1)$$

q_{max} being the q value of the observed maximum. By this approximation we estimated ~5.4 nm average *core-to-core* SNPs separation along both axes (q_z and q_y). According to the radius of a nanoparticle (~1.5 nm) obtained from SAXS and the estimated *core-to-core* separation, then the *edge-to-edge* inter-NPd should be ~2.4 nm. This suggests that each Au core is surrounded by slightly more than 1 TOA$^+$ monolayer accounting for a fully extended *all-trans* configuration (0.11−0.13 nm between CH_2)[49] along the C8 alkyl chain (~1.0 nm). However, this is a low estimate since TOA$^+$ chains are open

DOI: 10.1021/jp511014q
J. Phys. Chem. C 2015, 119, 5098−5106

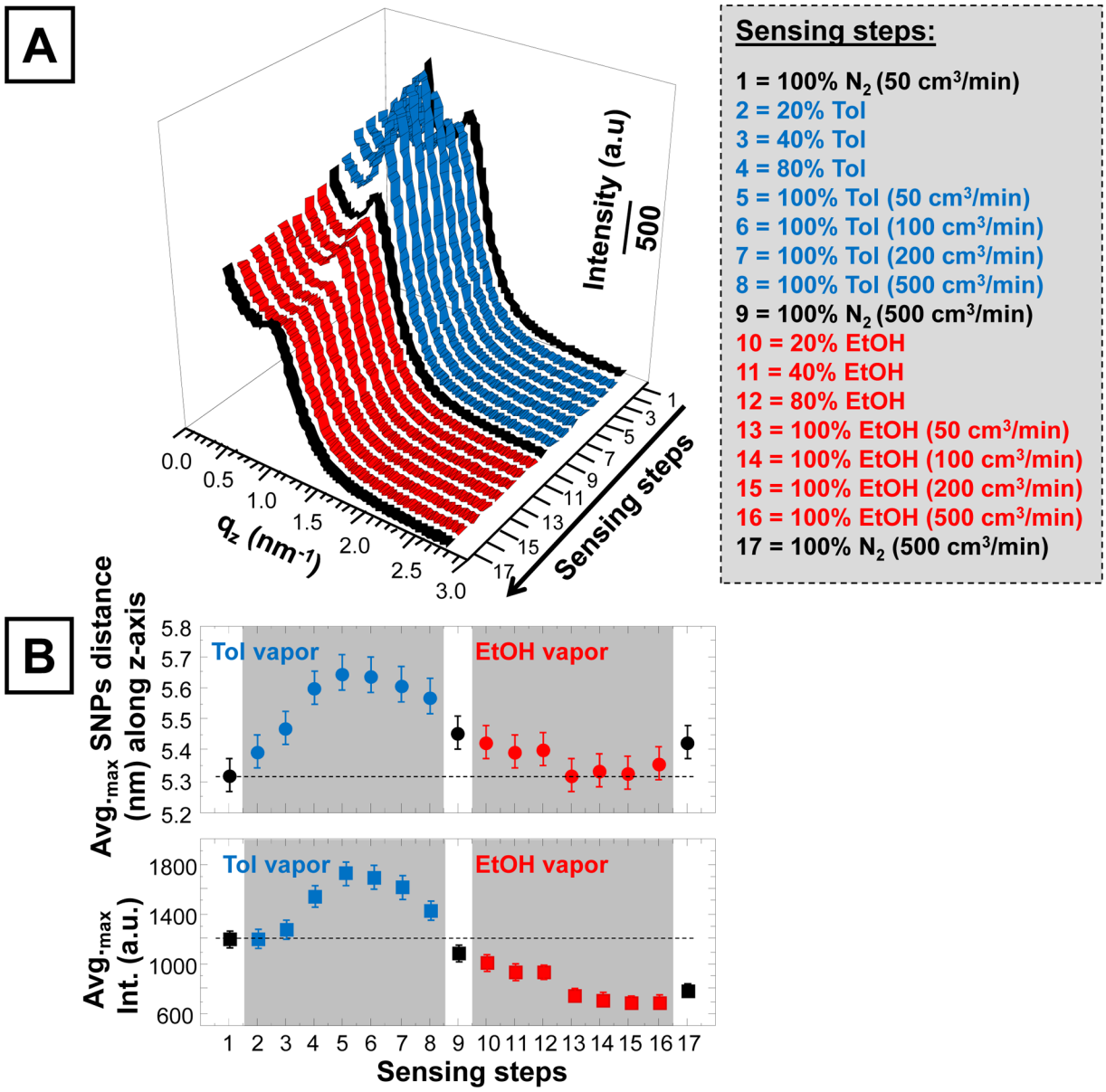

Figure 2. *In situ* GISAXS (q_z versus intensity) performed on a selected as-formed SNPs film subjected to increasing concentration and flow of Tol and EtOH as indicated in each step (A). The plot below shows average maximum (Avg_{max}) intensity and *core-to-core* distance along the *z*-axis (derived from q_z values) change upon each step as indicated (B).

and not as well packed as MPCs. Recent small-angle X-ray diffraction (SAXRD) experiments performed on Au MPCs of various sizes and chain lengths exhibited ∼1.7 nm *edge-to-edge* separation measured for solid-state 1-decanethiol (C10S) Au MPCs film.[36] A shorter distance (∼1.7 nm) than the sum of two C10S chains (∼2.0 nm) indicates some degree of interdigitation between alkyl chains.[40] The distance between SNPs exceeded the length of two surfactant chains (∼2.4 nm), suggesting the presence of a third TOA^+ chain (*vide infra*). This configuration fits well only if there is some degree of interdigation between the three TOA^+ chains.

Changes in Nanoparticles Distance and Film Structure upon VOCs. Figure 2A shows *in situ* GISAXS evolution plots along the *z*-axis (perpendicular to the substrate sample) for a single as-formed SNPs film exposed to N_2 and increasing concentration of toluene (Tol) and ethanol (EtOH) as indicated (see experimental GISAXS sensing setup in Scheme S3). Figure 2B shows a plot of an average *core-to-core* inter-NPd versus average maximum intensity (at q_{max}) along with standard deviation obtained from each experimental step as indicated. Both peak position and intensity provide quantitative and qualitative information about inter-NPd and film structure, respectively. Interestingly, GISAXS evolution shows distinct behavior for the same film toward nonpolar and polar vapors. An increasing concentration of Tol vapor causes an increase in SNPs distance and intensity, whereas in EtOH the film never restructures back and inter-NPd seems to be slightly affected. According to Guinier[41] and assuming a film composed of spherical NPs with spatial correlation, two variables can increase GISAXS intensity: (a) an increase in packing factor (at fixed q) and (b) increase in distance between NPs. Our experimental results show just ∼0.4 nm SNPs separation and a large ∼30% increase in intensity at 80% Tol vapor. This suggests that the increase in intensity should be associated with

DOI: 10.1021/jp511014q
J. Phys. Chem. C 2015, 119, 5098−5106

an increase in packing density rather than an increase in inter-NPd.[42] This somehow opposes the behavior of organic-coated Pt_2Cu_3 NPs[24] whose intensity profile readily decreases (broaden) upon exposure to hexane and increases back once all vapor has evaporated from the film. In conclusion, our film changes from a correlated into a more correlated (more ordered) structure as soon as Tol vapor partition into the film. It should be mentioned that just ∼0.4 nm increase in distance upon high concentration of Tol is intriguing since, for instance, Wan et al.[36] showed ∼3× larger increase (∼1.5 nm) separation for a C12S Au MPCs film exposed to similar Tol vapor concentrations (75%). Here, we noticed again striking differences between films composed of surfactant- and monolayer-protected Au NPs. As-formed surfactant-coated NPs initially exhibit a sort of poor correlation, which improves as soon as Tol partitions into the film. In the absence of Tol (100% N_2) the film slowly restructures and SNPs closely returns to its initial stage.

A different paradigm is observed when the film is exposed to EtOH. First, there is almost no inter-NPd change between the initial stage at 100% N_2 (before Tol, step 9) and the film at high EtOH vapor concentration (steps 13−16) considering that changes fall within the standard deviation. Second, there is small distance shrinkage between SNPs (∼0.1−0.2 nm) at saturated EtOH vapor with respect to before EtOH (step 9). It should recall that is the same film exposed to alternating cycles of N_2, Tol, and EtOH. Last, if we compare step 1 with step 17, then SNPs distance (q_z) and intensity (at $q_{z,max}$) never return to their initial position indicating film irreversibility. The apparent decrease in intensity (see Table S1) can be associated with the loss of SNPs correlation within the film. Although not discussed by Fang and co-workers,[24] in their report there is a noticeable broadening and decrease in peak intensity during vapor exposure, which corresponds to the stage where the film losses some correlation. In summary, the decreased intensity along with peak broadening is consistent with a decrease in packing density and, as a consequence, a decrease of SNPs correlation. On the other hand, film irreversibility may be assigned to persistent molecular forces between alkyl chains[34] and/or potential H-bonding between metallic cores.[37,43] Figure S4 shows an *in situ* GISAXS plot obtained along the *y*-axis (parallel to the substrate sample), indicating a similar sensing behavior upon Tol and EtOH vapors. Table S1 summarizes all the results obtained from the as-formed sample shown in Figure 2. SAXS experiments performed on a drop-casted SNPs film exposed to Tol and EtOH solvents exhibit qualitatively similar results to those obtained by GISAXS as shown in Figure S5 (Supporting Information).

Film Flexibility. In order to explore into the importance of the organic coating composition toward film flexibility in VOCs sensors, as-formed SNPs were liquid-phase place-exchanged with nonanedithiol (C9S2H2) (NDT) followed by exposure to saturated Tol vapor (100%). Figure 3 shows *in situ* GISAXS evolution plots along the *z*-axis of a selected as-treated film exposed to Tol as indicated. Table 1 shows results along *y*- and *z*-axis from the sample shown in Figure 3. The GISAXS plot and table show neglectable changes in distance and film structure upon saturated Tol, suggesting that dithiols constrained mobility between NPs thus preventing further film restructuring. Interestingly, Table 1 shows an increase in NPs distance along both axes after NDT treatment. At the interface (parallel to the substrate) the inter-NPd increased from ∼5.4 to ∼6.7 nm (∼1.3 nm) whereas along the *z*-axis the increase was

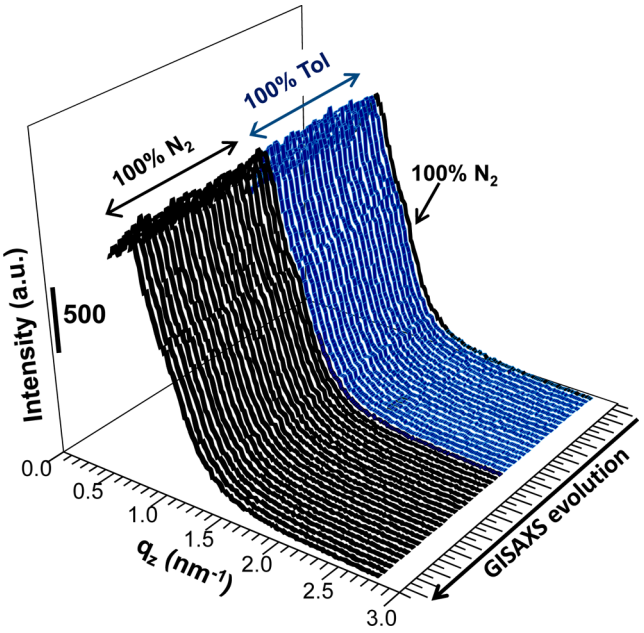

Figure 3. *In situ* GISAXS (q_z versus intensity) performed on a selected NDT-treated film exposed to alternating 100% N_2 and 100% Tol vapor (at the higher flux, 500 $cm^3 \cdot min^{-1}$) and back to N_2 as indicated.

relatively larger ∼2.0 nm, leading to a final *core-to-core* separation of ∼7.4 nm. Interestingly, SAXS experiments also revealed similar inter-NPd increase (∼7.5 nm, see Table 2) after NDT treatment. These results suggest that NDT ligands exchanged/interacted more effectively along the perpendicular axis (away from the interface). This is consistent with the assumption that SNPs within the film are more exposed away from the interface. Binding of HS−$(R)_n$−SH groups to the surface of two adjacent Au cores is expected to cause cross-linkage if separation between them is similar to the incoming alkyl chain length. Since the initial distance between SNPs is too large (∼2.4 nm), relative to the dithiol length (∼1.0 nm), and the incorporation of NDT increased even more the inter-NPd, we ruled out cross-linking. Although the NDT treatment seemed to greatly reduce film flexibility,[14,44] the source of film constrain remains unknown. It is possible that the organic composition and the adopted alkyl chain structure around the Au core could play a determining role in film flexibility and NPs separation (vide infra).

Alkyl Chain Chemistry and Structure after Dithiols Exchange. As a first approach, we performed XPS experiments using Mg Kα source on as-treated films, but unfortunately we observed a significant signal attenuation likely caused by large amounts of detergent and relatively low sensitivity of S 2p level for this excitation energy. To overcome this impediment, we performed X-ray absorption near-edge spectroscopy (XANES) at the S K-edge for both as-treated films using S Kα X-ray fluorescence signal. Figure 4A shows XANES spectra obtained from (NDT)- and C9SH (NT)-treated SNPs film (see Experimental Section for more details). The film exchanged with NDT exhibits two broad bands at ∼2480 and ∼2472 eV corresponding to S−Au and S−C resonances, respectively. However, the NT-treated film exhibits just one intense band at the S−C interaction. Previous XANES studies performed on various sizes hexanethiolate-coated (C6S) Au MPCs suggested two possible reasons for explaining the different intensities as follows.[45] One is attributed to molecular distortions that change

DOI: 10.1021/jp511014q
J. Phys. Chem. C 2015, 119, 5098−5106

Table 1. Summarized GISAXS Results from the As-Treated Sample Shown in Figure 3

	NDT-treated film	q max (nm^{-1})	Intensity (a.u.)	*core-to-core* distance (nm)[b]	Δ d (nm)[c]	Δ Intensity (a.u.)[d]	Δ Intensity %[e]	*edge-to-edge* distance (nm)[f]
along q_y	Initial	0.84	1218	6.7	/	/	/	3.7
	Tol vapor (step 15)[a]	0.82	1258	6.8	0.1	40	3	3.8
	Final	0.84	1109	6.7	0.0	-109	-9	3.7
along q_z	Initial	0.75	1382	7.5	/	/	/	4.5
	Tol vapor (step 15)[a]	0.75	1416	7.5	0.0	34	2	4.5
	Final	0.75	1322	7.5	0.0	-60	-4	4.5

[a]Maximum change in q during Tol vapor sensing. [b]The *core-to-core* distance between nanoparticles using eq 1. [c]Distance difference between the indicated step with respect to initial step. [d]Intensity difference between the indicated step and the initial step. [e]Intensity percent change in this step with respect to intensity at initial step. [f]The *edge-to-edge* distance was calculated according to the radius of a SNP (~1.5 nm) obtained from SAXS.

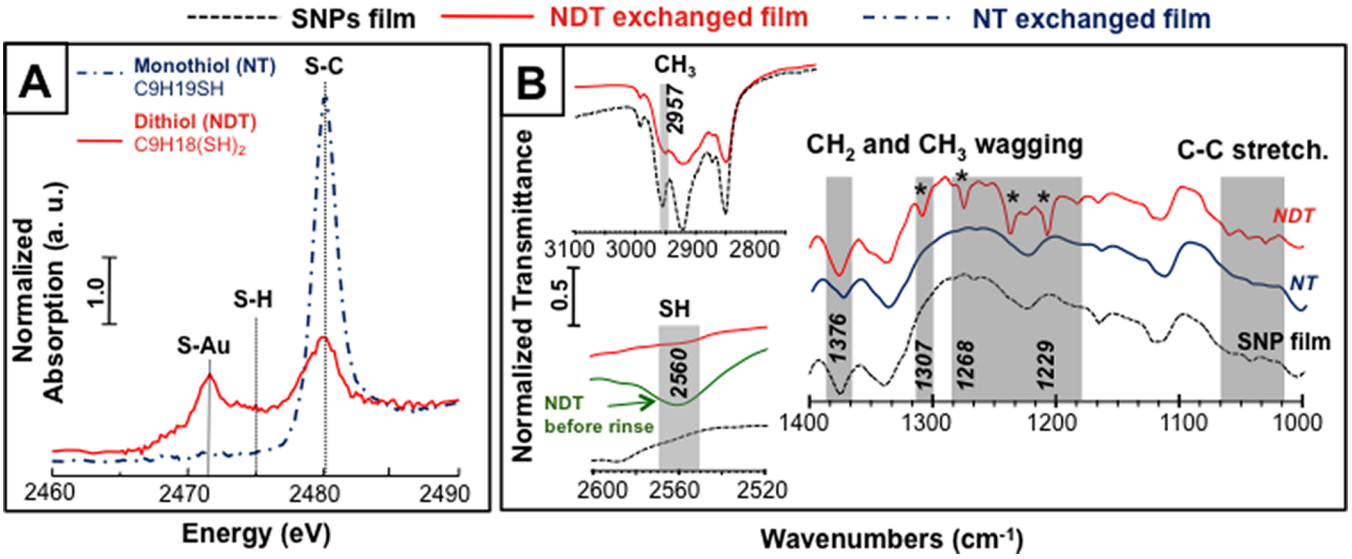

Figure 4. XANES (a) and FT-IR (b) spectra taken from NDT- and NT-treated SNPs films washed with hexane unless indicated. SNP films employed in FT-IR were thiol exchanged in the vapor phase in order to avoid nanoparticles detaching from the film. Plots are offset for better comparison. Note: an asterisk indicates new forming bands.

the final orbital state, while the other could be associated with NPs size and their ability to be S-enriched/depleted at the Au surface. In order to explore further, we performed fluorescence experiments to measure the S:Au atomic ratio for those thiol-treated films. Our results indicated almost 2 orders of magnitude smaller S:Au ratio (0.0046) with respect to chemically synthesized C6S Au MPCs of similar size which exhibited ~2 Au per single S atom (ratio ~0.47).[45] The small number of S atoms suggests that a large amount of surfactant, likely in the form of a micelle, prevented to some extent the R−S−Au interaction. Also, molecular distortions may be playing a determining role. At this point, we are unsure about which contribution predominates; however, the disappearance and absence of peaks at 2560 cm^{-1} and ~2475 eV observed by FT-IR results (*vide infra*) and XANES, respectively, indicate that free thiols are readily removed after hexane rinsing. Since XANES shows the presence of S−C groups after rinsing, it is reasonable to think that molecular distortions may be responsible for the absence of the S−Au peak. It should be noted that peak positions at Au−S and Au−C from the NDT-treated film remained unmodified which excludes new forming (i.e., S−S dimerization) or breaking bonds (i.e., C−S bond).

Figure 4B shows three different FT-IR spectra taken between 3000−2800, 2600−2500, and 1400−1100 cm^{-1} assigned to C−H stretching, S−H, and CH_2 and CH_3 wagging vibrations along with C−C stretching, respectively. All FT-IR bands were normalized with respect to the peak at ~1375 cm^{-1} named umbrella (U) mode and used as a yardstick because is essentially insensitive to any structural change suffered by any other CH group along the alkyl chain.[34] The SNPs film was exchanged with NT and NDT vapors followed by copious rinsing with hexane unless indicated. It should be mentioned that NDT and NT exchange was performed in the vapor phase in order to avoid SNPs detaching from the film during the exchange reaction. By FT-IR experiments we look into the appearance/disappearance, increase/decrease intensity, and shift in wavenumbers of the alkyl-chain-containing groups.[18,40,46] The first apparent change is indicated by a significant decrease of the CH_3 asymmetric and CH_2 asymmetric stretching bands at 2957 and ~2929 cm^{-1}, respectively, indicating that some CH_3 head groups and TOA^+ ligands were replaced and removed, respectively, by the incoming R−SH groups.[46] It is particularly interesting the appearance of new peaks (marked with an asterisk in the figure) between 1180 and 1380 cm^{-1} assigned to twisting-rocking and

DOI: 10.1021/jp511014q
J. Phys. Chem. C 2015, 119, 5098−5106

Table 2. Qualitative and Quantitative Results Obtained from As-Formed and NDT-Treated SNPs Film Exposed to Vapors and Liquid Tol and EtOH; Measurements Were Obtained by Additional Techniques Including SAXS, FT-IR, UV−Vis (Plasmon), and Cyclic Voltammetry (CV) Indicated as Film Current (See Figure S9)

		GISAXS[a]					SAXS[b]		
		core-to-core distance parallel (q_y, nm^{-1})	*core-to-core* distance perpendicular (q_z, nm^{-1})	Δd_y (nm)	Δd_z (nm)	correlation	*core-to-core* distance (nm)	Δd (nm)	correlation
SNPs film	Initial	5.4	5.3	/	/	regular	6.5	/	poor
	Tol	5.7	5.6	0.3	0.3	good	7.3	0.8	good
	Initial	5.5	5.5	/	/	regular	6.5	/	poor
	EtOH	5.4	5.3	-0.1	-0.1	bad	7.1*	0.6	good
NDT exchanged film	Initial	6.7	7.5	/	/	regular	7.5	/	regular
	Tol	6.8	7.5	0.1	0.0	regular	7.3	-0.2	regular

		FTIR (film[a] in vapor[c])		SNPs film[b] current		UV-vis (film[a] in vapor[c])		UV-vis (film in solvent)	
		CH_2 asym. peak (cm^{-1})	alkyl chain structure[d]	Cyclic voltammetry	%Response (%R)[e]	Plasmon (λ, nm)	Plasmon shift (Δλ, nm)	λ (nm)	Δλ (nm)
SNPs film	Initial	2923[Ref.18]	disordered[Ref.18]	capacitive/ionic 3.0 10^{-9} A	/	538.2[Ref.18]	/	545.0[Ref.18]	/
	Tol	2930[Ref.18]	disordered[Ref.18]	small increase[Ref.15]	1x	536.6[Ref.18]	-1.6[Ref.18]	560.0 (red)[Ref.18]	15.0[Ref.18]
	EtOH	2921[Ref.18]	ordered[Ref.18]	large increase[Ref.15]	~4x (than Tol)[f]	541.6[Ref.18]	3.4[Ref.18]	565.0 (red)[Ref.18]	20.0[Ref.18]
NDT exchanged film	Initial	2922	ordered w/r to intial	ohmic 1.4 10^{-8} A	/	574.5	/	564.6	/
	Tol	NR	NC	NR	/	NR	NR	NR	17.0

[a]As-formed film. [b]Drop-cast deposited SNPs film. [c]Film exposed to headspace vapors. [d]Alkyl chain order based on gauche defects observed at the CH_2 asymmetric stretching band. [e]% response = $(i_r - i_b)/i_b \times 100\% = \Delta i/i_b \times 100\%$, where i_r and i_b corresponds to current response and baseline, respectively. [f]Indicates that %*R* to EtOH is ~4 times larger than Tol at saturated vapor concentration; (w/r) = with respect to; (NC) = no change; (NR) = not run. [*]Note that inter-NPd increases in the presence of EtOH solvent. The source is unknown.

wagging progression bands for NDT-treated films. Snyder[47] determined two different kinds of defects in the region between 1300 and 1400 cm^{-1} corresponding to (a) C−H gauche defects at the end and root of the alkyl chain and (b) an internal defect named "kink" located at the center. Importantly, we can ensure the existence of an internal kink since the band at 1307 cm^{-1} is accompanied by another band at 1337 cm^{-1} of similar intensity.[34] Finally, the bands between 1020 and 1080 cm^{-1} can be assigned to C−C stretching modes, which seems to slightly change after NDT treatment. So far, these results clearly suggest that the small number of exchanged dithiol chains adopted a particular structure at the Au surface. On the other hand, it has been shown that long dithiols tend to oxidize in the form of disulfides (S−S) between two or more alkyl chains.[48] Therefore, one may consider two possible alkyl chain conformations: (a) two or more dithiol chains linked by strong S−S bonding or (b) both R−SH groups, from the same chain, formed thiolates at the surface of a single Au NP. Since XANES experiments excluded bonds breaking or forming, we can rule out the former structure. UV−vis results shown in Figure S6 of SNPs films exchanged with NT and NDT in the vapor phase excludes the possibility of cross-linking between Au NPs. Finally, consistent with XANES, the peak at 2560 cm^{-1} corresponding to free thiols disappeared after copious rinsing with hexane.

In summary, our results shed light on the importance of the organic coating composition and conformation around the Au core toward film flexibility and inter-NPd, respectively. Scheme S7 (Supporting Information) represents that a small number of NDT molecules reached the Au surface adopting a loop conformation according to XANES and FT-IR results, respectively. Table 2 shows a summary of all the results obtained here along with results from the literature[15,18] for as-prepared and as-treated SNPs films exposed to vapors and solvents as indicated. Columns exhibit all the additional techniques, besides GISAXS, employed for exploring all the films involved in this work.

■ CONCLUSION

In conclusion, SNPs films formed by immersion exhibited short-range correlation and ~5.4 nm *core-to-core* separation, which is a larger distance when compared to well-assembled monolayer-protected clusters of similar core size. The large SNPs separation was attributed to excess amount of weakly coordinated TOA^+ ligands around the Au nanoparticle. Importantly, GISAXS experiments determined an increase in inter-NPd distance and improved film correlation during increasing concentrations of Tol vapor. The increase in distance is consistent with coupling effects in LSPR sensor as indicated by a blue-shift of the plasmon maximum (see Table 2). On the other hand, the same film exposed to EtOH exhibited a slight decrease in distance between SNPs and loss of film structure as noted by the decrease in the intensity peak.

DOI: 10.1021/jp511014q
J. Phys. Chem. C 2015, 119, 5098−5106

The slight decrease in distance could be associated with the significant red-shift and alkyl chain restructuring as indicated by LSPR and FT-IR, respectively.[18] Ibañez and Zamborini[15] suggested that electron transport in surfactant-coated NPs films primarily occurred via ionic currents, which were favored by the presence of polar vapors (i.e., EtOH) over nonpolar ones as noted by the large increase in current (Table 2). Consistent with the above, the current response to Tol is 4× smaller relative to EtOH at same vapor concentrations, indicating that two sensing mechanisms may compete with each other: ionic currents versus electron hopping. Whereas the former exhibited a significant increase in current, the latter commonly shows a decrease in current (increase resistance) due to an increase in distance between SNPs (film swelling). Changes in inter-NPd were mainly attributed to film flexibility provided by the large amount of surfactant ligands. Once dithiol molecules replaced/removed some TOA^+ groups, film flexibility was severely diminished, limiting NPs mobility and film restructuring. After dithiol treatment we observed two interesting aspects: (a) inter-NPd increased and (b) dithiols interacted more favorably with SNPs located away from the interface in the film. FT-IR exhibited kink defects suggesting that alkanedithiols may form a loop around the Au cores, which could be responsible for further inter-NPd separation. The lack of response upon saturated Tol for dithiol-treated films remains unknown; however, we believe that the significant removal of soft ligands (i.e., TOA^+) prevented NPs mobility. Interestingly, CV curves exhibit a change from ionic to ohmic film current after dithiol exchange (Figure S8). We will perform solid-state NMR in order to gain more details about each carbon along the dithiol chain. Finally, this work demonstrated that an organic-coated film is an interesting platform for exploring the role of the organic coating and its effects on nanoparticles distance and film structure upon sensing polar and nonpolar VOCs.

■ ASSOCIATED CONTENT

Supporting Information

SAXS fitted curves of SNPs film dispersed in toluene, SAXS plot of drop-cast deposited SNPs on mica, representation of the experimental sensing setup, *in situ* GISAXS along the *y*-axis of SNPs film exposed to increasing concentrations of Tol and EtOH vapors, table showing GISAXS results along the *y*-axis and *z*-axis, SAXS data showing SNPs film immersed into EtOH and Tol solutions, UV−vis of SNP films treated with NDT and NT, scheme of SNPs before and after exchange with dithiols, CV plots before and after dithiol exchange. This material is available free of charge via the Internet at http://pubs.acs.org.

■ AUTHOR INFORMATION

Corresponding Author

*Phone +54 (221) 425 7430/7296; fax +54 (221) 425 4642; e-mail fjiban@inifta.unlp.edu.ar (F.J.I.).

Notes

The authors declare no competing financial interest.

■ ACKNOWLEDGMENTS

We gratefully acknowledge financial support from projects PICT-PRH 295 and International Cooperation Projects (CONICET-NSF) with Dr. Zamborini at the University of Louisville. This work was partially supported by Brazilian Synchrotron Light Laboratory (Proposal XRD1-14440), Brazil, and CONICET (PIP 201101-01035), Argentina.

■ REFERENCES

(1) Liao, H.-C.; Tsao, C.-S.; Lin, T.-H.; Jao, M.-H.; Chuang, C.-M.; Chang, S.-Y.; Huang, Y.-C.; Shao, Y.-T.; Chen, C.-Y.; Su, C.-J.; et al. Nanoparticle-Tuned Self-Organization of a Bulk Heterojunction Hybrid Solar Cell with Enhanced Performance. *ACS Nano* **2012**, *6*, 1657−1666.

(2) Lee, K.; Irudayaraj, J. Correct Spectral Conversion between Surface-Enhanced Raman and Plasmon Resonance Scattering from Nanoparticle Dimers for Single-Molecule Detection. *Small* **2013**, *9*, 1106−1115.

(3) Ibañez, F. J.; Zamborini, F. P. Chemiresistive Sensing with Chemically Modified Metal and Alloy Nanoparticles. *Small* **2012**, *8*, 174−202.

(4) Zamborini, F. P.; Leopold, M. C.; Hicks, J. F.; Kulesza, P. J.; Malik, M. A.; Murray, R. W. Electron Hopping Conductivity and Vapor Sensing Properties of Flexible Network Polymer Films of Metal Nanoparticles. *J. Am. Chem. Soc.* **2002**, *124*, 8958−8964.

(5) Zamborini, F. P.; Smart, L. E.; Leopold, M. C.; Murray, R. W. Distance-Dependent Electron Hopping Conductivity and Nanoscale Lithography of Chemically-Linked Gold Monolayer Protected Cluster Films. *Anal. Chim. Acta* **2003**, *496*, 3−16.

(6) Mie, G. Beiträge Zur Optik Trüber Medien, Speziell Kolloidaler Metallösungen. *Ann. Phys.* **1908**, *330*, 377−445.

(7) Wohltjen, H.; Snow, A. W. Colloidal Metal-Insulator-Metal Ensemble Chemiresistor Sensor. *Anal. Chem.* **1998**, *70*, 2856−2859.

(8) Snow, A. W.; Ancona, M. G.; Park, D. Nanodimensionally Driven Analyte Response Reversal in Gold Nanocluster Chemiresistor Sensing. *Langmuir* **2012**, *28*, 15438−15443.

(9) Steinecker, W. H.; Rowe, M. P.; Zellers, E. T. Model of Vapor-Induced Resistivity Changes in Gold-Thiolate Monolayer-Protected Nanoparticle Sensor Films. *Anal. Chem.* **2007**, *79*, 4977−4986.

(10) Krasteva, N.; Besnard, I.; Guse, B.; Bauer, R. E.; Müllen, K.; Yasuda, A.; Vossmeyer, T. Self-Assembled Gold Nanoparticle/Dendrimer Composite Films for Vapor Sensing Applications. *Nano Lett.* **2002**, *2*, 551−555.

(11) Wang, L.; Luo, J.; Yin, J.; Zhang, H.; Wu, J.; Shi, X.; Crew, E.; Xu, Z.; Rendeng, Q.; Lu, S.; et al. Flexible Chemiresistor Sensors: Thin Film Assemblies of Nanoparticles on a Polyethylene Terephthalate Substrate. *J. Mater. Chem.* **2010**, *20*, 907−915.

(12) Leopold, M. C.; Donkers, R. L.; Georganopoulou, D.; Fisher, M.; Zamborini, F. P.; Murray, R. W. Growth, Conductivity, and Vapor Response Properties of Metal Ion-Carboxylate Linked Nanoparticle Films. *Faraday Discuss.* **2004**, *125*, 63−76.

(13) Yvonne Joseph, I. B. Self-Assembled Gold Nanoparticle/Alkanedithiol Films: Preparation, Electron Microscopy, XPS-Analysis, Charge Transport, and Vapor-Sensing Properties. *J. Phys. Chem. B* **2003**, *107*, 7406−7413.

(14) Joseph, Y.; Peie, A.; Chen, X.; Michl, J.; Vossmeyer, T.; Yasuda, A. Vapor Sensitivity of Networked Gold Nanoparticle Chemiresistors: Importance of Flexibility and Resistivity of the Interlinkage. *J. Phys. Chem. C* **2007**, *111*, 12855−12859.

(15) Ibañez, F. J.; Zamborini, F. P. Chemiresistive Sensing of Volatile Organic Compounds with Films of Surfactant-Stabilized Gold and Gold-Silver Alloy Nanoparticles. *ACS Nano* **2008**, *2*, 1543−1552.

(16) Chen, Y.-Q.; Lu, C.-J. Surface Modification on Silver Nanoparticles for Enhancing Vapor Selectivity of Localized Surface Plasmon Resonance Sensors. *Sens. Actuators, B* **2009**, *135*, 492−498.

(17) Cheng, C.-S.; Chen, Y.-Q.; Lu, C.-J. Organic Vapour Sensing Using Localized Surface Plasmon Resonance Spectrum of Metallic Nanoparticles Self Assemble Monolayer. *Talanta* **2007**, *73*, 358−365.

(18) Dalfovo, M. C.; Salvarezza, R. C.; Ibañez, F. J. Improved Vapor Selectivity and Stability of Localized Surface Plasmon Resonance with a Surfactant-Coated Au Nanoparticles Film. *Anal. Chem.* **2012**, *84*, 4886−4892.

(19) Scholten, K.; Reddy, K.; Fan, X.; Zellers, E. T. Vapor Discrimination by Dual-Laser Reflectance Sensing of a Single Functionalized Nanoparticle Film. *Anal. Methods* **2013**, *5*, 4268−4272.

(20) Potyrailo, R. A.; Larsen, M.; Riccobono, O. Detection of Individual Vapors and Their Mixtures Using a Selectivity-Tunable

DOI: 10.1021/jp511014q
J. Phys. Chem. C 2015, 119, 5098−5106

Three-Dimensional Network of Plasmonic Nanoparticles. *Angew. Chem., Int. Ed.* **2013**, *52*, 10360−10364.
(21) García-Berríos, E.; Gao, T.; Woodka, M. D.; Maldonado, S.; Brunschwig, B. S.; Ellsworth, M. W.; Lewis, N. S. Response versus Chain Length of Alkanethiol-Capped Au Nanoparticle Chemiresistive Chemical Vapor Sensors. *J. Phys. Chem. C* **2010**, *114*, 21914−21920.
(22) Zhang, H.-L.; Evans, S. D.; Henderson, J. R.; Miles, R. E.; Shen, T.-H. Vapour Sensing Using Surface Functionalized Gold Nanoparticles. *Nanotechnology* **2002**, *13*, 439−444.
(23) Goodfellow, B. W.; Korgel, B. A. Reversible Solvent Vapor-Mediated Phase Changes in Nanocrystal Superlattices. *ACS Nano* **2011**, *5*, 2419−2424.
(24) Zhang, J.; Luo, Z.; Martens, B.; Quan, Z.; Kumbhar, A.; Porter, N.; Wang, Y.; Smilgies, D.-M.; Fang, J. Reversible Kirkwood−Alder Transition Observed in Pt_3Cu_2 Nanoctahedron Assemblies under Controlled Solvent Annealing/Drying Conditions. *J. Am. Chem. Soc.* **2012**, *134*, 14043−14049.
(25) Wan, Y.; Portalès, H.; Goubet, N.; Mermet, A.; Pileni, M.-P. Impact of Nanocrystallinity Segregation on the Growth and Morphology of Nanocrystal Superlattices. *Nano Res.* **2013**, *6*, 611−618.
(26) Bian, K.; Choi, J. J.; Kaushik, A.; Clancy, P.; Smilgies, D.-M.; Hanrath, T. Shape-Anisotropy Driven Symmetry Transformations in Nanocrystal Superlattice Polymorphs. *ACS Nano* **2011**, *5*, 2815−2823.
(27) Connolly, S.; Fullam, S.; Korgel, B.; Fitzmaurice, D. Time-Resolved Small-Angle X-Ray Scattering Studies of Nanocrystal Superlattice Self-Assembly. *J. Am. Chem. Soc.* **1998**, *120*, 2969−2970.
(28) Corricelli, M.; Depalo, N.; Fanizza, E.; Altamura, D.; Giannini, C.; Siliqi, D.; Di Mundo, R.; Palumbo, F.; Kravets, V. G.; Grigorenko, A. N.; et al. Two-Dimensional Plasmonic Superlattice Based on Au Nanoparticles Self-Assembling onto a Functionalized Substrate. *J. Phys. Chem. C* **2014**, *118*, 7579−7590.
(29) Wan, Y. F.; Goubet, N.; Albouy, P. A.; Pileni, M. P. Hierarchy in Au Nanocrystal Ordering in Supracrystals: A Potential Approach to Detect New Physical Properties. *Langmuir* **2013**, *29*, 7456−7463.
(30) Choi, J. J.; Bealing, C. R.; Bian, K.; Hughes, K. J.; Zhang, W.; Smilgies, D.-M.; Hennig, R. G.; Engstrom, J. R.; Hanrath, T. Controlling Nanocrystal Superlattice Symmetry and Shape-Anisotropic Interactions through Variable Ligand Surface Coverage. *J. Am. Chem. Soc.* **2011**, *133*, 3131−3138.
(31) Wang, Z.; Schliehe, C.; Bian, K.; Dale, D.; Bassett, W. A.; Hanrath, T.; Klinke, C.; Weller, H. Correlating Superlattice Polymorphs to Internanoparticle Distance, Packing Density, and Surface Lattice in Assemblies of PbS Nanoparticles. *Nano Lett.* **2013**, *13*, 1303−1311.
(32) Fink, J.; Kiely, C. J.; Bethell, D.; Schiffrin, D. J. Self-Organization of Nanosized Gold Particles. *Chem. Mater.* **1998**, *10*, 922−926.
(33) Abbate, M.; Vicentin, F. C.; Compagnon-Cailhol, V.; Rocha, M. C.; Tolentino, H. The Soft X-Ray Spectroscopy Beamline at the LNLS: Technical Description and Commissioning Results. *J. Synchrotron Radiat.* **1999**, *6*, 964−972.
(34) Hostetler, M. J.; Stokes, J. J.; Murray, R. W. Infrared Spectroscopy of Three-Dimensional Self-Assembled Monolayers: N-Alkanethiolate Monolayers on Gold Cluster Compounds. *Langmuir* **1996**, *12*, 3604−3612.
(35) Correlation refers to the probability to find a spatial distribution of entities (NPs) in a certain volume. The neighbor-to-neighbor distance is defined by "*d*". As the probability to find more objects separated equal distances "*d*" increases, the larger the increase in *q* (scattering) intensity and the larger the "correlation".
(36) Wan, Y.; Goubet, N.; Albouy, P.-A.; Schaeffer, N.; Pileni, M.-P. Hierarchy in Au Nanocrystal Ordering in a Supracrystal: II. Control of Interparticle Distances. *Langmuir* **2013**, *29*, 13576−13581.
(37) Salzemann, C.; Zhai, W.; Goubet, N.; Pileni, M.-P. How to Tune the Au Internanocrystal Distance in Two Dimensional Self-Ordered Superlattices. *J. Phys. Chem. Lett.* **2010**, *1*, 149−154.
(38) Klecha, E.; Ingert, D.; Pileni, M. P. How the Level of Ordering of 2d Nanocrystal Superlattices Is Controlled by Their Deposition Mode. *J. Phys. Chem. Lett.* **2010**, *1*, 1616−1622.
(39) Guinier, A. *Small-Angle Scattering of X-rays*; John Wiley: New York, 1955.
(40) Terrill, R. H.; Postlethwaite, T. A.; Chen, C.-H.; Poon, C.-D.; Terzis, A.; Chen, A.; Hutchison, J. E.; Clark, M. R.; Wignall, G.; Londono, J. D.; et al. Monolayers in Three Dimensions: NMR, SAXS, Thermal, and Electron Hopping Studies of Alkanethiol Stabilized Gold Clusters. *J. Am. Chem. Soc.* **1995**, *117*, 12537−12548.
(41) Rice, S. A. Small Angle Scattering of X-rys. *J. Polym. Sci.* **1956**, *19*, 594.
(42) Sakka, S. *Handbook of Sol-Gel Science and Technology. 1. Sol-Gel Processing*; Springer: Berlin, 2005; Vol. *1*.
(43) Godfrey Alig, A. R.; Akbulut, M.; Golan, Y.; Israelachvili, J. Forces between Surfactant-Coated ZnS Nanoparticles in Dodecane: Effect of Water. *Adv. Funct. Mater.* **2006**, *16*, 2127−2134.
(44) Ibañez, F. J.; Gowrishetty, U.; Crain, M. M.; Walsh, K. M.; Zamborini, F. P. Chemiresistive Vapor Sensing with Microscale Films of Gold Monolayer Protected Clusters. *Anal. Chem.* **2006**, *78*, 753−761.
(45) Ramallo-López, J. M.; Giovanetti, L. J.; Requejo, F. G.; Isaacs, S. R.; Shon, Y. S.; Salmeron, M. Molecular Conformation Changes in Alkylthiol Ligands as a Function of Size in Gold Nanoparticles: X-Ray Absorption Studies. *Phys. Rev. B* **2006**, *74*, 073410.
(46) Choo, H.; Cutler, E.; Shon, Y.-S. Synthesis of Mixed Monolayer-Protected Gold Clusters from Thiol Mixtures: Variation in the Tail Group, Chain Length, and Solvent. *Langmuir* **2003**, *19*, 8555−8559.
(47) Snyder, R. G. Vibrational Study of the Chain Conformation of the Liquid N-Paraffins and Molten Polyethylene. *J. Chem. Phys.* **1967**, *47*, 1316−1360.
(48) Millone, M. A. D.; Hamoudi, H.; Rodríguez, L.; Rubert, A.; Benítez, G. A.; Vela, M. E.; Salvarezza, R. C.; Gayone, J. E.; Sánchez, E. A.; Grizzi, O.; et al. Self-Assembly of Alkanedithiols on Au(111) from Solution: Effect of Chain Length and Self-Assembly Conditions. *Langmuir* **2009**, *25*, 12945−12953.
(49) Porter, M. D.; Bright, T. B.; Allara, D. L.; Chidsey, C. E. D. Spontaneously Organized Molecular Assemblies. 4. Structural Characterization of N-Alkyl Thiol Monolayers on Gold by Optical Ellipsometry, Infrared Spectroscopy, and Electrochemistry. *J. Am. Chem. Soc.* **1987**, *109*, 3559−3568.

DOI: 10.1021/jp511014q
J. Phys. Chem. C 2015, 119, 5098−5106